JACS
JOURNAL OF THE AMERICAN CHEMICAL SOCIETY
COMMUNICATION
pubs.acs.org/JACS

4D Scanning Ultrafast Electron Microscopy: Visualization of Materials Surface Dynamics

Omar F. Mohammed,[†] Ding-Shyue Yang,[†] Samir Kumar Pal,[‡] and Ahmed H. Zewail[*,†]

[†]Physical Biology Center for Ultrafast Science and Technology, Arthur Amos Noyes Laboratory of Chemical Physics, California Institute of Technology, Pasadena, California 91125, United States

[‡]Department of CBMS, UNANST, S.N. Bose National Center for Basic Sciences, Kolkata 700 098, India

ABSTRACT: The continuous electron beam of conventional scanning electron microscopes (SEM) limits the temporal resolution required for the study of ultrafast dynamics of materials surfaces. Here, we report the development of scanning ultrafast electron microscopy (S-UEM) as a time-resolved method with resolutions in both space and time. The approach is demonstrated in the investigation of the dynamics of semiconducting and metallic materials visualized using secondary-electron images and backscattering electron diffraction patterns. For probing, the electron packet was photogenerated from the sharp field-emitter tip of the microscope with a very low number of electrons in order to suppress space−charge repulsion between electrons and reach the ultrashort temporal resolution, an improvement of orders of magnitude when compared to the traditional beam-blanking method. Moreover, the spatial resolution of SEM is maintained, thus enabling spatiotemporal visualization of surface dynamics following the initiation of change by femtosecond heating or excitation. We discuss capabilities and potential applications of S-UEM in materials and biological science.

The applications of four-dimensional ultrafast electron microscopy (4D UEM)[1,2] have now spanned various areas of study, ranging from materials science to biological imaging.[1,3] This methodology utilizes ultrashort electron pulses, synchronized with optical pulses, for imaging the object after electrons transmit the specimen. Whereas the primary electron beam and Bragg diffraction are the main signals detected in UEM-1 and UEM-2 in this laboratory,[1] in scanning UEM (S-UEM) we detect secondary electrons (SE), backscattered electrons (BSE), and electron backscattering diffraction (EBSD) of Kikuchi bands, as shown previously for static imaging.[4] By so doing, it is possible to study the morphological, physical, and chemical dynamics of surfaces.

The advantages of S-UEM are several. First, thick or bulk specimens can be examined, reducing the effort in sample preparation, a feature that is attractive in many studies. Moreover, unlike the thin specimens used in the transmission mode, thick samples provide a heat sink for experiments involving a temperature jump. The bulk of the specimen may also significantly reduce the radiation damage by laser and/or electrons. Second, because of the spatiotemporal resolutions, the sensitivity is suited for the study of surfaces and interfaces, including adsorbates. Third, unlike other methods that require compensation of the velocity mismatch between electrons and photons,[5] here this mismatch in arrival times is typically 100 fs for a footprint of only micrometer size. Finally, S-UEM is equipped with environmental and low-voltage-imaging capabilities, opening up possibilities for investigation of reactive surfaces and biological systems.

In this Communication, we report the first time-resolved imaging and diffraction achieved by S-UEM using in situ femtosecond excitation of various materials. In crystalline silicon, following 515-nm excitation, we were able to visualize carrier excitation dynamics at the surface, which we also used to characterize the resolution capability of S-UEM. The temporal resolution is 4 orders of magnitude better than that of the nanosecond-scale beam-blanking techniques[6] and is not limited by the response time (10-ps scale) of spectroscopic cathodoluminescence.[7] In the imaging mode, several additional materials were investigated: InAs, CdTe, and CdSe; metal surfaces such as aluminum, copper, bismuth, and calcium; and films of CdSe quantum dots (3.4-nm diameter) with or without TiO_2 (25 nm) particles, and other composites. In the diffraction mode, we observed the dynamics in the Kikuchi bands which result from the BSE near the surface region of the (InAs) single crystal. These studies highlight some of the capabilities unique to S-UEM, especially when comparing the results with those obtained in steady-state imaging[8] or by spectroscopic techniques.[9]

The concept involved in S-UEM imaging is illustrated in Figure 1. Here the focus is on real-time dynamics, and details of the instrumentation and operation modes can be found elsewhere.[4] Briefly, the output of a femtosecond fiber laser system was integrated with a modified SEM. The laser delivers IR pulses whose wavelength centers at 1030 nm and can be operated at variable repetition rates from 200 kHz to 25.4 MHz. The fundamental output was frequency-doubled, directed with precision through a pyrometric window, and tightly focused onto the cooled Schottky field-emitter tip (∼500 K) to photogenerate electron (probe) pulses which were then accelerated in a 30 kV voltage. For the present study, the residual IR beam was frequency-doubled (515 nm), separated by a dichroic mirror, and then directed and tightly focused (with a full width of ∼25 μm at $1/e$ of the maximum intensity) in situ onto the specimen at an incidence angle of ∼50° relative to the surface normal. A computer-controlled optical delay line was used to define the time axis of the frames recorded.

In the scan imaging mode of S-UEM, typically a dwell time of 1 μs was used at each probing location to enable different stroboscopic recording of images. The scanning takes place over

Received: April 5, 2011
Published: May 03, 2011

ACS Publications © 2011 American Chemical Society

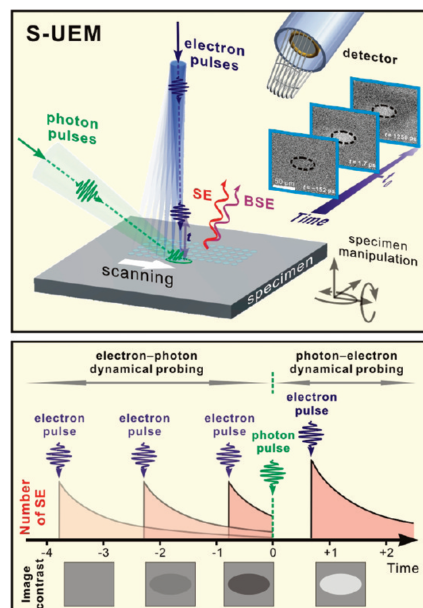

Figure 1. The concept of S-UEM (schematic) and the two regimes of probing. When the electron pulse is used for probing, it is spatially scanned over the surface of the specimen. For a fixed delay time, a frame of the image or diffraction is recorded. The resulting secondary electrons (SE) and/or backscattered electrons (BSE) from the excited or nonexcited regions are collected by the detector for imaging. In the lower panel, we display the expected temporal and contrast change of the image in the two regimes of interest.

both the laser-irradiated and the unexcited regions, and SE images are constructed after the emitted electrons are collected by a positively biased Everhart–Thornley detector. For diffraction, scanning is no longer needed, and EBSD patterns were recorded by a highly sensitive digital camera. All single-crystalline wafers used in this study were purchased from MTI Corp.

By delaying the arrival time of the initiating pulse with respect to the electron pulse, one can obtain a series of snapshots (frames) at well-defined times. The zero of time between the two pulses was first crudely estimated by calculating the travel distance for the optical and electron pulses after taking into account the speed difference; at 30 keV, the speed of electrons is one-third that of photons. However, an in situ and precise determination is required, and for this reason we imaged the charge distribution of surfaces while scanning the time delay, as described below.

Shown in Figure 2a is the dynamical change of single-crystal silicon observed using SE imaging, after referencing the frames to one taken at a negative time when the electron pulse arrives prior to the optical pulse (unexcited configuration). Immediately before time zero, no change is seen in the difference image, indicating the return of the specimen back to the equilibrated state and showing the reversibility of scanning in the stroboscopic experiments of imaging. In contrast, immediately after time zero (i.e., the arrival of the clocking pulse, t_0), the intensity of SE increases, only in the laser-irradiated region, signifying an elevated efficiency in the SE generation as a result of the femtosecond optical excitation.

These experiments thus provide the spatiotemporal dynamics on different time scales. The SE intensity of crystalline silicon at the center of the laser excitation footprint is plotted in Figure 2b as a function of the delay time (t) with 267-fs steps and up to

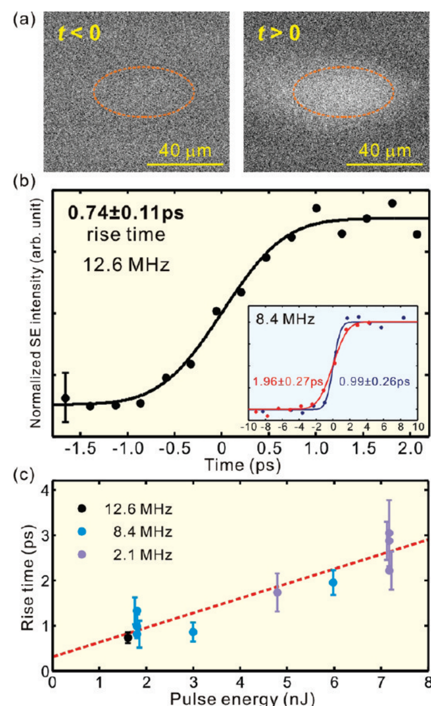

Figure 2. Dynamics of crystalline silicon and S-UEM temporal characteristics. (a) Contrast-enhanced difference of the SE images, referenced to a negative time frame, immediately before and after $t = 0$, at negative (left) and positive (right) times. The dashed ellipse indicates the location where the laser fluence falls to $1/e$ of the maximum at the center. (b) SE intensity change at the center of the excited region as a function of time, obtained using different repetition rates and laser fluences (see text). The solid lines are fits to an error function of the dynamics. (c) Rise time acquired from the silicon specimen, obtained at different repetition rates, as a function of the apparent optical pulse energy used to generate electron pulses. The dashed line is a linear fit.

2.1 ps; the apparent excitation fluence is ~0.5 mJ/cm^2 at the specimen. As can be seen, the time-dependent change of silicon after excitation occurs with a rise time of 740 ± 110 fs, when the energy of the electron-generating pulse was E_{emitter} = 1.4 nJ. This observation indicates no significant space–charge repulsion between electrons when the pulse contains a small number of electrons, the "single-electron regime".[1] On the other hand, the inset of Figure 2b displays the time-dependent change of silicon, and, from the fit to an error function, $1 + \text{erf}[(t - t_0)/\tau]$, we obtained the rise time at different E_{emitter}: 0.99 ± 0.26 ps for 1.6 nJ (blue), corresponding to an apparent fluence (F_{emitter}) of 1.8 mJ/cm^2, and 1.96 ± 0.27 ps at 5.3 nJ (red), corresponding to F_{emitter} = 6.0 mJ/cm^2; the fluence was obtained from knowledge of reflectivity and other beam properties. The increase in the rise time as the number of electrons in the pulse increases[10] illustrates the importance of single-electron imaging. Finally, the nearly linear relationship shown in Figure 2c for this dependence gives an intercept of ~0.3 ps in the limit of very low fluence, which agrees well with the theoretical calculation for electrons having ~0.8 eV of excess energy above the work function of the emitting tip.[10]

The observed surface phenomenon, i.e., the change in image contrast with time, can be understood as follows. When silicon, with an indirect band gap of 1.12 eV, is excited by the clocking green optical pulse (2.41 eV), an interband carrier transition takes place, and some electrons are promoted from the valence

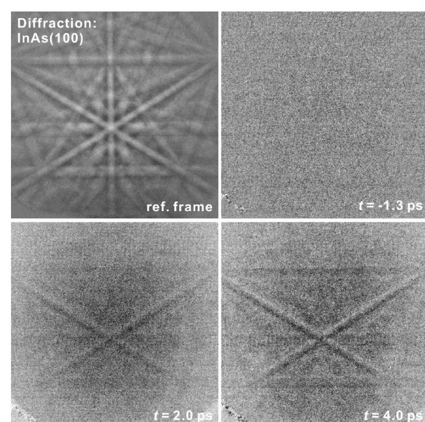

Figure 3. Time-resolved electron backscattering diffraction (EBSD) of single-crystal InAs(100). Differences in the diffraction pattern at selected times are referenced to a negative time frame (upper left). Note that not all Kikuchi bands show a dynamical change, reflecting the direction of atomic motions (see text). It can also be seen that the lattice dynamics undergoes further development after 2 ps (lower left and right).

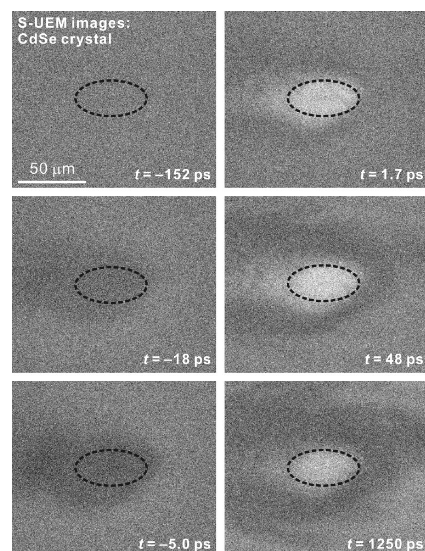

Figure 4. Image dynamical change of single-crystal CdSe(0001) at selected frame times. The dashed ellipses indicate the locations for $1/e$ of the maximum laser fluence used. No observable change at very negative time signifies the recovery of the system to an equilibrated state after each pump−probe event (upper left panel). The evolution of dark and bright contrast is discussed in the text.

band to the conduction band. As a result, it is easier energetically for these excited electrons to have a higher probability of SE emission. Moreover, conduction electrons resulting from excitation beneath the surface could contribute to enhancement of the contrast, because the acquired energy increases the effective escape depth to the surface, hence increased SE.[11]

With S-UEM, we also obtained time-resolved electron diffraction patterns, which can provide direct information on structural dynamics, similar to that provided by ultrafast electron diffraction for atomic-distance changes[12] or lattice contraction/expansion in materials.[2] Figure 3 displays the EBSD patterns of single-crystal InAs(100) as a function of time. A rapid increase in the diffraction difference is observed on the time scale of a few picoseconds. Such a difference pattern of adjacent black and white bands is principally the result of vertical shifts of the corresponding Kikuchi bands. The lattice expansion is along the surface normal direction, as supported by the absence of change for the vertical band. We estimate a lattice constant increase of 0.16% at t = 4 ps, which corresponds to a temperature rise of ∼350 K if the expansion is of a thermal nature (expansion coefficient of 4.52×10^{-6} °C^{-1}). However, given the heat capacity and other properties of InAs,[13] the maximum temperature jump would be ∼40 K at our fluence of ∼0.4 mJ/cm^2. Consistent with previous studies,[14] the uniaxial lattice expansion is, therefore, driven by the initial carriers' excitation and subsequent emission and thermalization of phonons. The lattice dynamics appears to be longer than the temporal resolution given in Figure 2b, also consistent with the latter being due to charge distribution and the former being controlled by nuclear motions following carrier excitation.[15]

One of the most significant applications of S-UEM is in the study of charge distribution on the nanometer scale at interfaces. For this reason we examined photoconductive semiconducting materials, which are important in optoelectronic devices, to demonstrate potential applications in this area of research. CdSe, with a direct band gap of 1.73 eV, is a prototype example; its charge dynamics on the nanometer length scale has been studied by spectroscopic methods,[16] and so are the effects of quantum confinement on photoconductivity[17] and electron injection and transport in the semiconducting thin film.[18] Considerable attention has been given to their use in electroluminescent devices.[19] In Figure 4, we present a series of SE difference images at selected times following the excitation of a CdSe(0001) single crystal. The contrast enhancement of SE emission at positive times, as in silicon, is due to the acquired energy of the excited carriers in the conduction band, as described before. However, in contrast with the dynamics of silicon, we also observed regions exhibiting suppression of contrast at negative times, and surrounding the excitation region within tens of micrometers at positive times.

The picture we have in mind is illustrated in the lower panel of Figure 1. There are two regimes of probing, one at positive times and the other at negative times. In the former case, the dynamics is initiated by the femtosecond optical pulse and probed by electrons, as described in the case of silicon (see Figure 2). In the latter regime (negative time), the pulsed primary electrons (30 keV) act as an excitation beam, followed by the laser probing pulse. The electron pump beam can generate secondary electrons (before the arrival of the laser pulse) from a region of relatively larger escape depth. Consequently, SE may result typically with a transient time on the picosecond to nanosecond time scale.[7] As the electron pulse marches toward t = 0, the number of SE decreases and image contrast darkens (see Figure 4). Thus, the laser pulse probes the relaxation of SE, due to either collision[20] with other particles (electrons/phonons) or radiative recombination (cathodoluminescence). We note that we have observed SE at negative time when the laser pulse was not present. It follows that the laser pulse is clocking the relaxation at negative time. Diffusion of excitons is expected to be on a time scale of tens to hundreds of picoseconds, for a diffusion constant on the order of 10 cm^2/s for CdSe,[21] and this may account for the spread of the dark contrast. It should be mentioned that no change was observed for SE detected when only the laser pulse was present for our ∼50 μJ/cm^2 photons, the transient field[22] is ineffective, as detailed elsewhere.

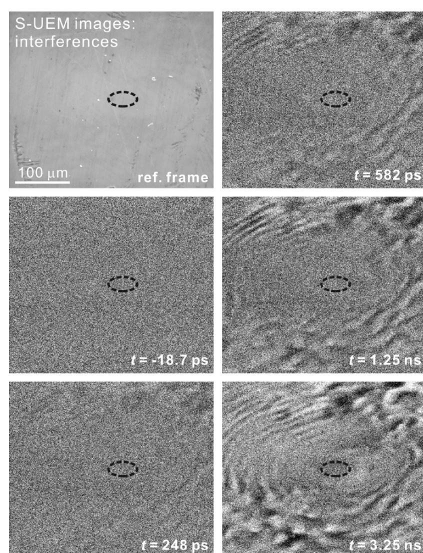

Figure 5. S-UEM images of aluminum surface displaying patterns of interference at longer times. The reference frame is indicated; the dashed ellipses give the location for $1/e$ of the maximum laser fluence used.

For metals, laser-induced periodic structures on surfaces have been studied at high laser fluences, ~0.35 J/cm^2.[23] However, all the patterns were imaged using time-averaged static microscopic methods, although the origin of the phenomena is believed to be dynamical in nature. On metal surfaces the patterns are thought to be formed from the interference between the incident light and the excited surface plasmons (SPs).[24] However, tungsten does not support SPs in the wavelength range of 240–920 nm, and the observation of a periodic structure for excitations at 400 and 800 nm[23] was recently concluded to be due to the competition of two ultrafast processes, electron–phonon coupling and hot-electron diffusion.[25]

In Figure 5, we present the surface interference pattern of aluminum as visualized using S-UEM. The effect is present only when both the electron and optical pulses are present. The change in the SE intensity was observed away from the laser-irradiated region and evolves slowly toward the center, in contrast with the behavior for the semiconducting materials discussed above. Similar transient patterns were also observed on the surface of copper, bismuth, and calcium, but for some materials, including cobalt, nickel, tungsten, gold, and stainless steel, such dynamics were not observed. This striking effect, which is a reflection of the plasmonic and magnonic properties of surfaces with roughness, is currently under further investigation.

In conclusion, the development of 4D scanning ultrafast electron microscopy promises to have wide-ranging applications in the study of surface materials with unprecedented spatiotemporal resolutions. Here, we highlight phenomena that relate to surface charge distribution, enhanced conductivity, and interference at surfaces of various materials. Future applications should take advantage of the ability to focus the electron beam so that catalytic sites can be explored[26] and enabling environmental microscopy[27] with new domains of resolutions. This capability and the low voltage of S-UEM may also provide an opportunity to study cathodoluminescence, charge transport in DNA systems,[28] and complex materials and biosystems under environmental conditions, with picoampere, not tens of nanoamperes as in SEM, electron imaging.

AUTHOR INFORMATION

Corresponding Author
zewail@caltech.edu

ACKNOWLEDGMENT

This work was supported by the NSF and the Air Force Office of Scientific Research in the Gordon & Betty Moore Physical Biology Center at Caltech. O.F.M. is grateful for a distinguished scholar award provided by the Arab Fund for Economic and Social Development. S.K.P. thanks Prof. Zewail for generous hospitality during the sabbatical stay.

REFERENCES

(1) Zewail, A. H. *Science* **2010**, *328*, 187.
(2) Zewail, A. H.; Thomas, J. M. *4D Electron Microscopy: Imaging in Space and Time*; Imperial College Press: London, 2010.
(3) Flannigan, D. J.; Barwick, B.; Zewail, A. H. *Proc. Natl. Acad. Sci. U.S.A.* **2010**, *107*, 9933.
(4) Yang, D.-S.; Mohammed, O. F.; Zewail, A. H. *Proc. Natl. Acad. Sci. U.S.A.* **2010**, *107*, 14993.
(5) Baum, P.; Zewail, A. H. *Proc. Natl. Acad. Sci. U.S.A.* **2006**, *103*, 16105.
(6) MacDonald, N. C.; Robinson, G. Y.; White, R. M. *J. Appl. Phys.* **1969**, *40*, 4516.
(7) Merano, M.; Sonderegger, S.; Crottini, A.; Collin, S.; Renucci, P.; Pelucchi, E.; Malko, A.; Baier, M. H.; Kapon, E.; Deveaud, B.; Ganiere, J. D. *Nature* **2005**, *438*, 479.
(8) Goldstein, J. I.; Newbury, D. E.; Joy, D. C.; Lyman, C. E.; Echlin, P.; Lifshin, E.; Sawyer, L.; Michael, J. R. *Scanning Electron Microscopy and X-Ray Microanalysis*, 3rd ed.; Springer: New York, 2003.
(9) Tanaka, T.; Harata, A.; Sawada, T. *J. Appl. Phys.* **1997**, *82*, 4033.
(10) Gahlmann, A.; Park, S. T.; Zewail, A. H. *Phys. Chem. Chem. Phys.* **2008**, *10*, 2894.
(11) Reimer, L. *Scanning Electron Microscopy: Physics of Image Formation and Microanalysis*, 2nd ed.; Springer: Berlin, 1998.
(12) Srinivasan, R.; Lobastov, V. A.; Ruan, C. Y.; Zewail, A. H. *Helv. Chim. Acta* **2003**, *86*, 1763.
(13) Levinshtein, M. E., Rumyantsev, S. L., Shur, M., Eds. *Handbook Series on Semiconductor Parameters*; World Scientific: Singapore, 1996.
(14) Yang, D.-S.; Gedik, N.; Zewail, A. H. *J. Phys. Chem. C* **2007**, *111*, 4889.
(15) Sundaram, S. K.; Mazur, E. *Nat. Mater.* **2002**, *1*, 217.
(16) Wang, F.; Shan, J.; Islam, M. A.; Herman, I. P.; Bonn, M.; Heinz, T. F. *Nat. Mater.* **2006**, *5*, 861.
(17) Makhal, A.; Yan, H. D.; Lemmens, P.; Pal, S. K. *J. Phys. Chem. C* **2010**, *114*, 627.
(18) Batabyal, S.; Makhal, A.; Das, K.; Raychaudhuri, A. K.; Pal, S. K. *Nanotechnology* **2011**, *22*, 195704.
(19) Colvin, V. L.; Schlamp, M. C.; Alivisatos, A. P. *Nature* **1994**, *370*, 354.
(20) Shih, A.; Yater, J.; Hor, C.; Abrams, R. *Appl. Surf. Sci.* **1997**, *111*, 251.
(21) Erland, J.; Razbirin, B. S.; Pantke, K. H.; Lyssenko, V. G.; Hvam, J. M. *Phys. Rev. B* **1993**, *47*, 3582.
(22) Schafer, S.; Liang, W. X.; Zewail, A. H. *Chem. Phys. Lett.* **2010**, *493*, 11.
(23) Vorobyev, A. Y.; Guo, C. L. *J. Appl. Phys.* **2008**, *104*, 063523.
(24) Bonchbruevich, A. M.; Libenson, M. N.; Makin, V. S.; Trubaev, V. V. *Opt. Eng.* **1992**, *31*, 718.
(25) Wang, J. C.; Guo, C. L. *J. Appl. Phys.* **2007**, *102*, 053522.
(26) Thomas, J. M.; Raja, R.; Lewis, D. W. *Angew. Chem., Int. Ed.* **2005**, *44*, 6456.
(27) Gai, P. L.; Boyes, E. D.; Helveg, S.; Hansen, P. L.; Giorgio, S.; Henry, C. R. *MRS Bull.* **2007**, *32*, 1044.
(28) Steckl, A. J. *Nat. Photon.* **2007**, *1*, 3.